Estuaries and Coasts (2018) 41:2056–2069
https://doi.org/10.1007/s12237-018-0372-0

Reconstructing Aragonite Saturation State Based on an Empirical Relationship for Northern California

Catherine V. Davis [1,2,3,4] · Kathryn Hewett [1,5] · Tessa M. Hill [1,4] · John L. Largier [1,5] · Brian Gaylord [1,6] · Jaime Jahncke [2]

Received: 31 July 2017 / Revised: 16 January 2018 / Accepted: 23 January 2018 / Published online: 13 April 2018

Abstract

Ocean acidification is a global phenomenon with highly regional spatial and temporal patterns. In order to address the challenges of future ocean acidification at a regional scale, it is necessary to increase the resolution of spatial and temporal monitoring of the inorganic carbon system beyond what is currently available. One approach is to develop empirical regional models that enable aragonite saturation state to be estimated from existing hydrographic measurements, for which greater spatial coverage and longer time series exist in addition to higher spatial and temporal resolution. We present such a relationship for aragonite saturation state for waters off Northern California based on in situ bottle sampling and instrumental measurements of temperature, salinity, and dissolved oxygen. Application of this relationship to existing datasets (5 to 200 m depth) demonstrates both seasonal and interannual variability in aragonite saturation state. We document a deeper aragonite saturation horizon and higher near surface aragonite saturation state in the summers of 2014 and 2015 (compared with 2010–2013), associated with anomalous warm conditions and decadal scale oscillations. Application of this model to time series data reiterates the direct association between low aragonite saturation state and upwelled waters and highlights the extent to which benthic communities on the Northern California shelf are already exposed to aragonite undersaturated waters.

Keywords Ocean acidification · Upwelling · California Current System · Aragonite saturation

Communicated by David Reide Corbett

Electronic supplementary material The online version of this article (https://doi.org/10.1007/s12237-018-0372-0) contains supplementary material, which is available to authorized users.

✉ Catherine V. Davis
cvdavis@seoe.sc.edu

[1] Bodega Marine Laboratory, University of California at Davis, 2099 Westshore Road, Bodega Bay, CA 94923, USA

[2] Point Blue Conservation Science, 3820 Cypress Dr. #11, Petaluma, CA 94954, USA

[3] Department of Earth & Planetary Sciences, University of California Davis, 1 Shields Ave, Davis, CA 95616, USA

[4] School of the Earth, Ocean, and Environment, University of South Carolina, Columbia, SC, USA

[5] Department of Environmental Science and Policy, University of California Davis, Davis, CA, USA

[6] Department of Evolution and Ecology, University of California Davis, 1 Shields Ave, Davis, CA 95616, USA

Introduction

The Earth is undergoing significant changes due to the anthropogenic input of carbon dioxide (CO_2) into the atmosphere. The oceans have, to date, absorbed a quarter to a third of these emissions (Canadell et al. 2007; Sabine et al. 2004; Sabine and Feely 2007), initiating an ongoing shift in marine chemistry known as "ocean acidification" or OA (Caldeira and Wickett 2003; Doney et al. 2009; Feely et al. 2004; Fabry et al. 2008; Feely et al. 2009; Kleypas et al. 1999; Orr et al. 2005; Sabine et al. 2004). While the surface ocean as a whole becomes more acidic and decreases in pH, the carbon system exhibits substantial spatial and temporal variability on regional scales (e.g., Alin et al. 2012; Feely et al. 2008; Hofmann et al. 2011; Juranek et al. 2009). These regional patterns overprint the global trend of OA (Kelly et al. 2013; Parker et al. 2011; Walther et al. 2010), and require an understanding of seasonal and interannual variability at a local level in order to monitor ongoing and anticipate future conditions in a more acidic ocean.

In the California Current System (CCS), deep waters already naturally rich in CO_2 are showing increased enrichment due to anthropogenic CO_2 as they upwell onto the continental shelf from central Canada to northern Mexico (e.g., Chan et al. 2017; Feely et al. 2008; Feely et al. 2016; Harris et al. 2013). Under these conditions, carbonate ion concentrations ($[CO_3^{2-}]$) within the water column are lower, creating a more stressful environment for shell-forming organisms that precipitate calcium carbonate structures. Moreover, evidence from recent decades and model projections suggests that rates and intensities of upwelling will continue to increase in the future (e.g., Bakun 1990; Bakun et al. 2015; Garcia-Reyes and Largier 2010; García-Reyes and Largier 2012; Sydeman et al. 2014; Varela et al. 2015; Wang et al. 2015; Snyder et al. 2003), although not all models agree and different regions may respond differently (Mote and Manuta 2002; Varela et al. 2015). Any increase in the strength or duration of upwelling intensity would increase organismal exposure to low $[CO_3^{2-}]$ waters in coastal upwelling regions (Gruber et al. 2012; Hauri et al. 2013). The interplay between these ongoing alterations in ocean chemistry and the regional dynamics of OA specific to the CCS highlight the need for higher-resolution OA monitoring in the CCS.

One important metric that can be used to quantify seawater conditions is aragonite saturation state (Ω_{arag}), defined as $\Omega_{arag} = [Ca^{2+}][CO_3^{2-}] / K_{sp}$, where $[Ca^{2+}]$ is the concentration of calcium cations and K_{sp} is a phase-specific, temperature-, and salinity-dependent constant. In general, Ω operates as a measure of the thermodynamic favorability of precipitation of a mineral, in this case of the aragonite crystalline form of calcium carbonate, with values $\Omega_{arag} < 1$ describing an aragonite undersaturated environment, where dissolution of aragonite shells is favored over precipitation. Although Ω_{arag} alone does not describe the entire marine inorganic carbonate system nor the full range of impacts on organisms, it is an often-used threshold for organismal response to OA.

At present, the paucity of existing OA measurements often impedes the use of Ω_{arag} as a useful index for characterizing local- and regional-scale carbonate system conditions. Most instrumental records suitable for determining Ω_{arag} span only years (in rare cases, decades), and therefore are of limited value for teasing apart interannual and decadal scale signals. These existing datasets are furthermore often confined to discrete locations or sampling stations. One solution for increasing both the temporal and spatial resolution of OA monitoring is the development of empirical models to estimate OA locally. These empirical models are based on more commonly recorded hydrographic properties such as temperature, salinity, and dissolved oxygen (DO). Such models have been successfully developed in both the Southern CCS by Alin et al. (2012) and the Northern CCS by Juranek et al. (2009), for use in estimating Ω_{arag}.

Here, we present a model for waters off Northern California that define a relationship for Ω_{arag} specific to the Central CCS, based on shipboard measurements of temperature, salinity, and DO, and laboratory measurements of pH and alkalinity to constrain Ω_{arag}. A second regional dataset was used to validate this relationship. The resultant relationship is compared to previous studies (Alin et al. 2012; Juranek et al. 2009) and applied to characterize key aspects of the regional spatial and temporal variability in Ω_{arag} along the Northern California shelf, in the Central CCS.

Methods

Study Region

The CCS includes the shallow (< 300 m), equatorward-flowing California Current (CC) and the poleward flowing California Undercurrent (CUC) with a core of maximum velocity between 100 and 300 m near the continental slope (Hickey, 1979; Lynn and Simpson 1987). The CC is fed by water masses from the North Pacific Current, characterized by relatively cold, less saline (33–34), oxygen-rich, nutrient-poor, and higher pH conditions (Pickard 1964; Reid et al. 1958). The CUC, by contrast, is fed by water masses originating from Pacific Equatorial Waters (PEW) and characterized by relatively warm, salty (> 34), oxygen-poor, nutrient-rich, and low pH conditions (Gay and Chereskin 2009; Hickey 1979; Huyer et al. 1998; Lynn and Simpson 1987; Pickard 1964; Sverdrup et al. 1942). As the CUC flows northward, warm and salty PEW waters mix with colder, less saline water masses from the subarctic North Pacific, which results in a progressive dilution of PEW (Thomson and Krassovski, 2010). This study focuses on the region inshore of the primary CC, where wind driven coastal upwelling brings colder, subsurface water to the surface (Fig. 1).

The CCS, like other Eastern Boundary Current Systems, includes a seasonal wind-driven coastal upwelling regime, which usually begins in early spring along the Northern California coast (García-Reyes and Largier 2012; Hickey 1998; Pennington and Chavez, 2000). This phenomenon is driven by strong, northwesterly winds that induce net transport of surface water offshore and cause the upwelling of deep, cold, nutrient-rich, oxygen-poor waters onto the continental shelf and into the euphotic zone. As deeper water masses in the North Pacific Ocean are naturally enriched in CO_2 (Broecker and Peng, 1982), they are additionally characterized by low pH and low carbonate saturation states (Alin et al. 2012; Fassbender et al. 2011; Feely et al. 2008; Hales et al. 2005; Juranek et al. 2009). Along the CCS, shelf waters originate from depths between 100 to 300 m during upwelling, with the core of the CUC located along isopycnals 26.4–26.6 kg m^{-3} (Gay and Chereskin, 2009; Lynn and Simpson 1987; Pierce et al. 2012). Prior studies

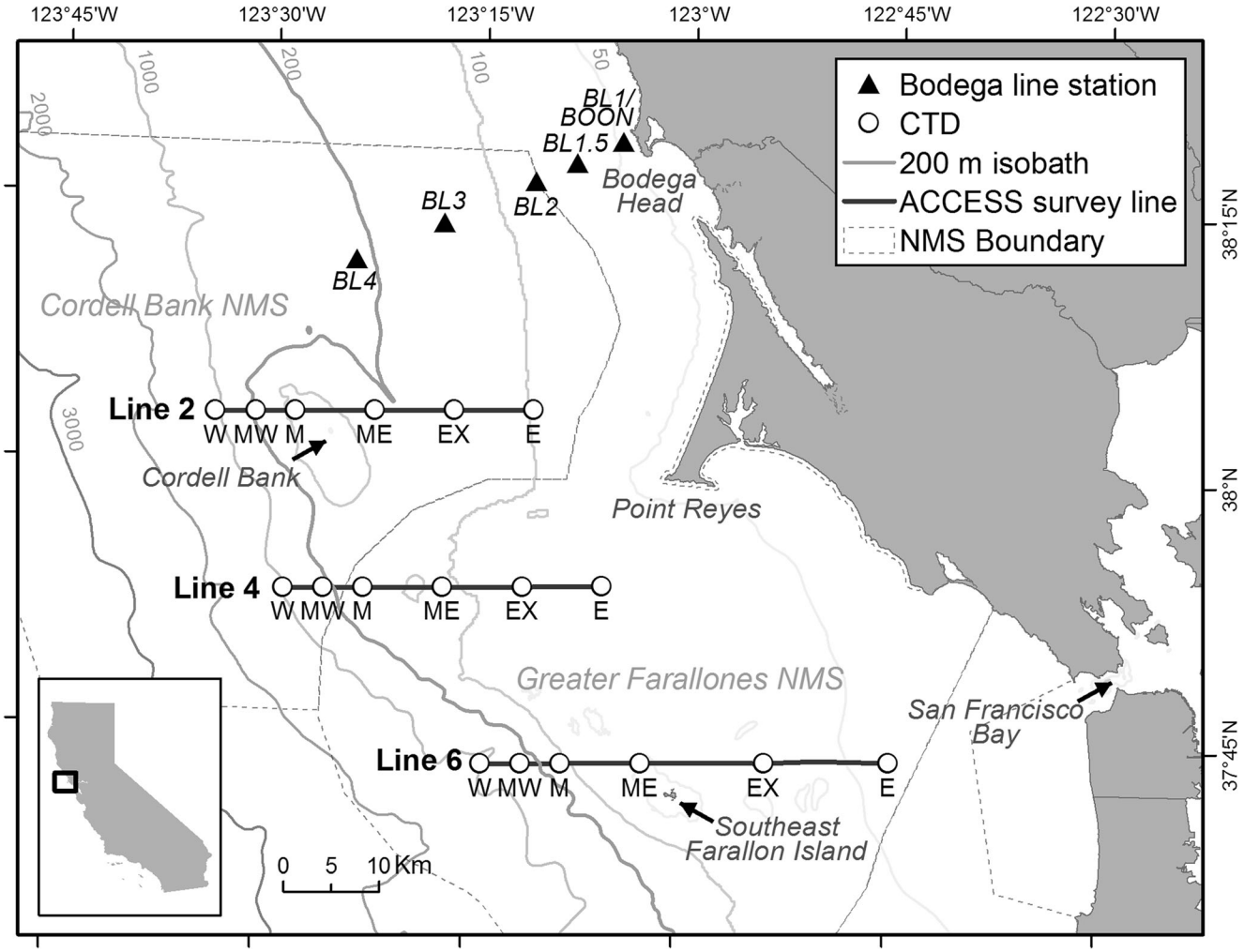

Fig. 1 Map of collection sites in the Gulf of the Farallones, over Cordell Bank and the regions directly offshore from Bodega Head, located within the California Current System. Stations sampled along the Bodega Line (BL) are shown in black, and transects sampled on ACCESS cruises are shown in white

identify the depth of the 26.0–26.2 kg m^{-3} isopycnal as a key derived variable within the CCS, with the Ω_{arag} saturation horizon at 26.2 kg m^{-3} (Feely et al. 2008).

As the strength and extent of coastal upwelling vary spatially and temporally along the CCS, coastal waters also experience a wide range of pH due to the varying relative influences of upwelled waters. For example, in 2013, the Bodega Ocean Observing Node (BOON; 38° 19.110′ N 123° 04.294′ W) offshore mooring recorded surface pH values ranging from 7.4 to 8.2 (total scale), a ~ 85% change in hydrogen ion ([H+]). Ongoing changes in the seasonality, duration, and intensity of upwelling along with the increasing influence of anthropogenic CO_2 on upwelled waters are likely to have wide-ranging effects on Eastern Boundary Current ecosystems such as the California Margin (García-Reyes et al. 2015), where benthic and planktic communities will be more frequently exposed to waters undersaturated with respect to aragonite.

Data Collection

Paired water samples and hydrographic measurements were collected on Applied California Current Ecosystem Studies (ACCESS) cruises from 2013 to 2015 and as part of the UC Davis Bodega Marine Laboratory (BML) "Bodega Line" cruises between 2012 and 2015. ACCESS sampling took place along five transects, from 37° N to 39° N, with efforts focused on the continental shelf (Fig. 1). Cruise transects were repeated up to three times annually between May and September onboard the R/V *Fulmar*. A conductivity-temperature-depth (CTD) profiler (Sea-Bird Electronics, SBE 19, equipped with a SBE 63 optical DO sensor) was used to obtain vertical profiles of temperature, salinity, and DO versus depth at up to six stations along each transect (Fig. 1). DO sensors were factory calibrated annually for an initial accuracy of ± 3 μmol/kg (~ 0.07 ml/L) or ± 2%. Discrete water samples were collected at the bottom of each

CTD profile for measurement of pH and total alkalinity. Water was collected from depths between 27 and 224 m using a 3-L Niskin bottle and immediately dispensed into duplicate 100 mL borosilicate glass bottles and preserved shipboard by the addition of mercuric chloride ($HgCl_2$). Additional samples were collected year-round from five on-shelf locations along the Bodega Line transect, at depths between 1 and 200 m, consistent with methods onboard ACCESS cruises (Fig. 1). Temperature, salinity, and DO measurements were also obtained from the BOON located at Bodega Line Station 1. This 32 m deep mooring is equipped with SBE microCAT and Precision Measurement Engineering (PME) miniDOT sensors at ~ 30 m depth. The miniDOT sensor has a reported accuracy of ± 10 μmol/kg or ± 5%.

Water Chemistry Analyses

Water samples were analyzed at BML spectrophotometrically for pH (total scale) using either a Sunburst SAMI (Submersible Autonomous Moored Instrument) modified for benchtop use (SD ± 0.009) or an Ocean Optics Jaz Spectrophotometer EL200 (SD ± 0.003) using *m*-cresol purple (Dickson et al. 2007). The SAMI was calibrated at Sunburst by determining molar absorbtivities specific to each batch. This was then corrected to Dickson CRM by pH measured and pH calculated from DIC. For samples run on the Jaz Spectrophotometer, a calibration regression was generated for each batch of dye and calibrated against Tris for a < 0.1 pH unit offset. Total alkalinity was run via automated Gran titration on a Metrohm 809 Titrando (SD ± 4.2 μmol/kg), with acid concentrations standardized to Dickson certified reference materials. Measurements of pH and total alkalinity were used together with CTD measurements of temperature and salinity to calculate Ω_{arag} using the software CO2calc (Robbins et al. 2010) with CO_2 equilibrium constants pK_1 and pK_2 from Millero (2010) and $KHSO_4$ from Dickson (1990).

Model Development and Evaluation

Relationships between Ω_{arag} and environmental variables were developed based on shipboard data from ACCESS cruises using R (R Core Team 2013), while holding the Bodega Line measurements in reserve for model validation. Stepwise regression was utilized in selecting predictive variables from shipboard measurements (temperature, salinity, DO, and depth), season, wind speed, and the Pacific Fisheries Environmental Laboratory (PFEL) upwelling index. Varying degrees of interactivity between parameters were tested and a best-fit model was selected based on a combination of Akaike Information Criterion (AIC), a frequently used tool for comparing candidate models based on maximum likelihood values (Akaike 1974), and fit to calculated values from both ACCESS and Bodega Line Data. Model validation was undertaken both by testing the model against Bodega Line data and by bootstrap resampling of the ACCESS dataset in which subsamples of our dataset were tested against our chosen model, as implemented in the R software package, "boot" (Fig. 2; Canty and Ripley 2016).

Results

Empirically Determined Model

We present a new regional relationship for Northern California shelf waters developed from data collected onboard ACCESS cruises between May and July, 2013–2015, months in which ocean conditions are dominated by wind-driven upwelling (Largier et al. 1993; García-Reyes and Largier 2012). The relationship includes temperature (T (°C)), salinity (S), and DO (μmol/kg), as well as interactions between the three variables (Eq. 1):

$$\begin{aligned}\Omega_{arag} = {} & \alpha_0 + \alpha_T(T) + \alpha_S(S) + \alpha_{DO}(DO) \\ & + \alpha_{TS}(T{*}S) + \alpha_{TDO}(T{*}DO) \\ & + \alpha_{DOS}(DO{*}S) + \alpha_{TSDO}(T{*}S{*}DO)\end{aligned} \quad (1)$$

where all α constants are shown in Table 1. Estimated values fit well to observed values ($R^2 = 0.92$, $p < 0.005$) with a root mean squared error of 0.09 and better predictive power shallower than 150 m (Fig. 2).

A simplified model requiring only salinity and DO was an equally good fit for ACCESS data and actually yielded the minimum AIC value:

$$\Omega_{arag} = \alpha_{02} + \alpha_{S2}(S) + \alpha_{DO2}(DO) + \alpha_{DOS2}(DO{*}S) \quad (2)$$

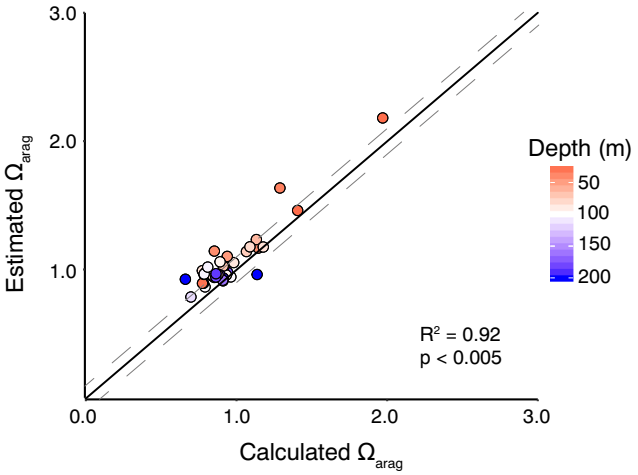

Fig. 2 Correlation between estimated and observed Ω_{arag} for samples taken onboard ACCESS cruises in 2013–2015, with deeper samples represented in blue and shallower samples in red. Ideal (1:1) fit is represented by the black line, with $\Omega_{arag} \pm 0.1$ shown in dashed gray lines

Table 1 Comparison between several models tested including the parameters included, constants and standard deviation, fit of the model to both the ACCESS data used for calibrations, and the Bodega Line dataset used for validation and the ΔAIC from the minimum AIC value achieved. Our favored model is in bold and should yield $\Omega_{arag} = 1$ when $T = 9$, $S = 33.8$, and DO = 105

Parameters	Constants ± standard deviation	R^2 fit to ACCESS	ΔAIC	R^2 fit to Bodega Line
S, DO, DO ∗ *S*	$\alpha_0 = -36.97997 \pm 6.65924$ $\alpha_S = 1.10990 \pm 0.19656$ $\alpha_{DO} = 0.40585 \pm 0.04478$ $\alpha_{DOS} = -0.01191 \pm 0.00133$	0.92	0	0.62
T, *S*, DO, *T* ∗ *S*, *T* ∗ DO, DO ∗ *S*, *T* ∗ *S* ∗ DO	$\alpha 0 = -222.7 \pm 132.2$ $\alpha T = 21.80 \pm 15.11e$ $\alpha S = 6.653 \pm 3.920$ $\alpha DO = 1.340 \pm 0.5434$ $\alpha TS = -0.6499 \pm 0.4484$ $\alpha TDO = -0.1121 \pm 0.06431$ $\alpha DOS = -0.03990 \pm 0.01621$ $\alpha TSDO = 0.003355 \pm 0.001920$	0.92	4	0.79
T, DO, DO ∗ *T*	$\alpha 0 = 2.2277895 \pm 0.6013926$ $\alpha T = -0.1691366 \pm 0.0658708$ $\alpha DO = -0.0131453 \pm 0.0030623$ $\alpha TDO = 0.0016624 \pm 0.0003009$	0.87	15	0.80

where all α constants are shown in Table 1. While the reduced number of inputs may make such a simplified model optimal for the ACCESS calibration dataset, it was found to be less predictive of the Bodega Line dataset during model validation (Table 1). Thus, Eq. 1 was deemed preferable for covering the region.

Model Validation

Model validation was achieved by two approaches. The first was bootstrap resampling of the ACCESS data used for model development, which with 500 iterations produced the highest frequency of R^2 values between 0.9 and 0.95 (Fig. 3). Our chosen model was also tested against independent data from the Bodega Line, which included higher Ω_{arag} values and lower salinities than observed in ACCESS cruise samples and resulted in a good fit ($R^2 = 0.79$, $p < 0.005$) with a slight bias towards overestimating Ω_{arag} (Fig. 3). Although the ACCESS data were limited to May through July samples, the resulting relationship was found to be applicable year-round to the Bodega Line data (1–200m water depth), with the exception of September, discussed further below.

Exclusion of September Data

During model development and validation, samples taken between August 20 and September 20 from both ACCESS and Bodega Line datasets in 2012–2015, referred to hereafter as "September," deviated from modeled relationships. All three model parameters (temperature, salinity, and DO) display a less robust linear relationship with observed Ω_{arag} values as compared to spring and early summer cruises (Fig. 4), and inclusion of September data consistently resulted in a worse model fit. September data were therefore excluded to produce a model that accurately estimates Ω_{arag} at other times. No modeling attempts based on September data exclusively produced reasonably predictive models ($R^2 < 0.56$, $p < 0.005$). Where model-inferred Ω_{arag} time series are presented here,

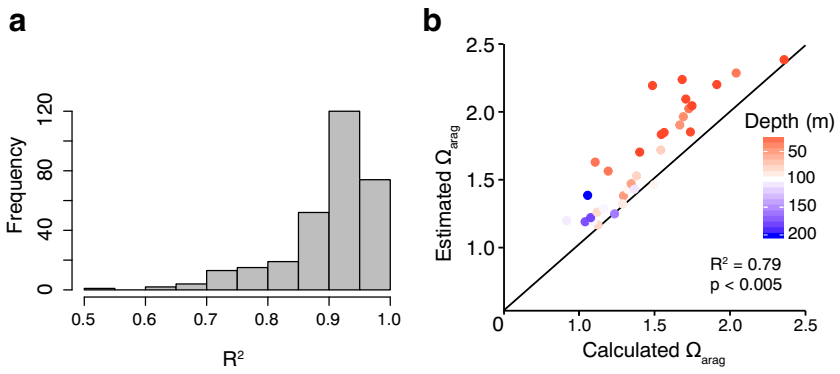

Fig. 3 Model verification by **a** bootstrap resampling of the ACCESS dataset, with a histogram of resulting R^2 values shown and **b** testing estimated and observed Ω_{arag} for samples taken along the Bodega Line (2012–2015). An ideal (1:1) fit is indicated by the black line

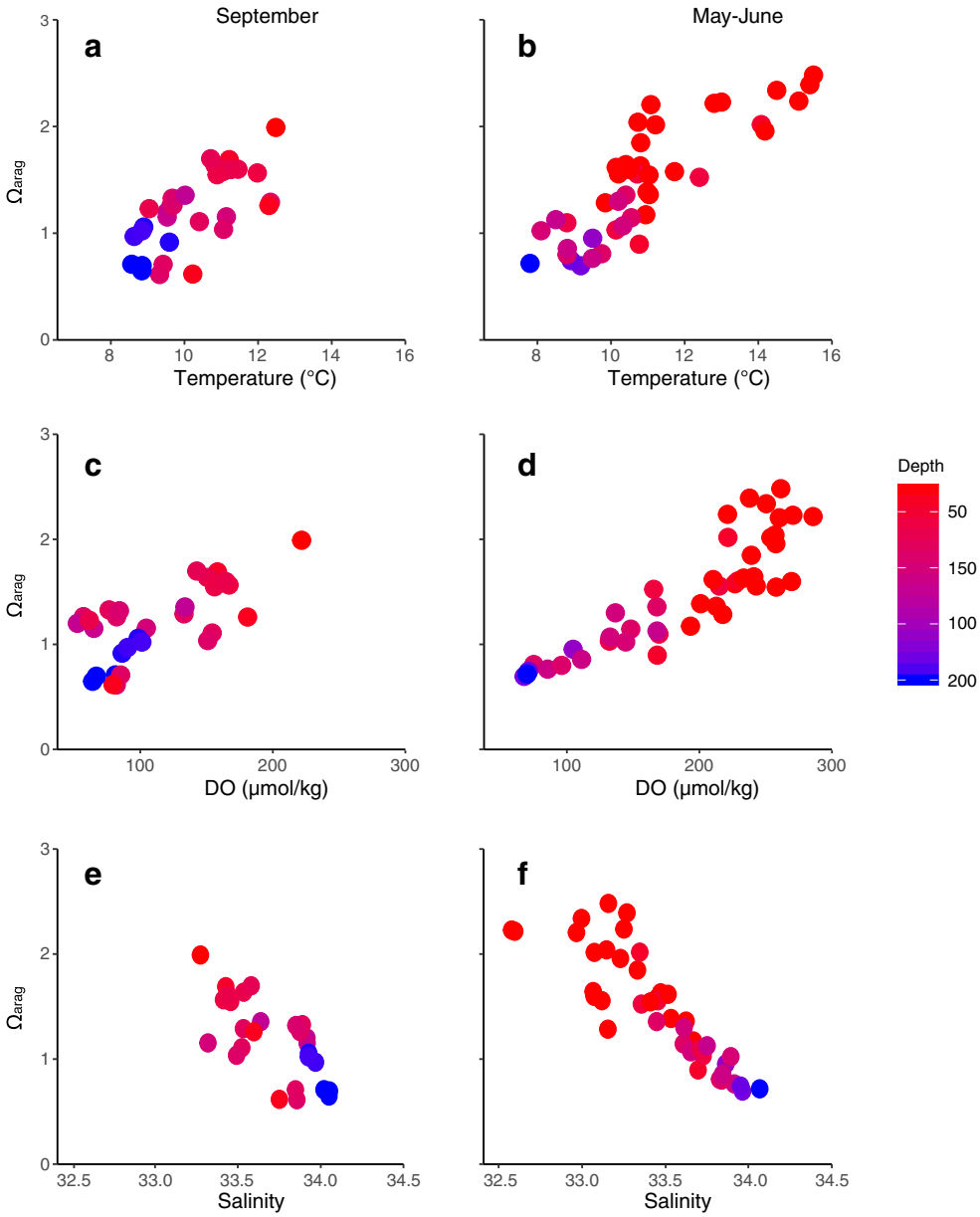

Fig. 4 Relationships between Ω_{arag} and temperature, DO, and salinity, respectively—based on ACCESS data (2013–2015). Relationships for September are compared with relationships for May–July. Panels **a**, **c**, and **e** show September values for Ω_{arag} as a function of temperature (R^2 = 0.45), DO ($R^2 = 0.48$), and salinity ($p > 0.05$), respectively. Panels **b**, **d**, and **f** show May–July values for Ω_{arag} as a function of temperature ($R^2 = 0.70$), DO ($R^2 = 0.72$), and salinity (R^2 = 0.20), respectively

September data has been identified, and while providing potentially valuable data in context, may not be as quantitatively robust. September data are discussed further in "The association of low Ω_{arag} with upwelled waters."

Comparison to Previously Published Models

Calculated Ω_{arag} values were compared to estimated values from other empirical relationships for the Northern and Southern CCS (Alin et al. 2012; Juranek et al. 2009). Both models provided a significant correlation but a notably poorer fit for ACCESS data: Juranek et al. (2009) model, $R^2 = 0.63$, $p < 0.005$; Alin et al. (2012) model, $R^2 = 0.59$, $p < 0.005$ (Fig. S1). The Alin et al. (2012) relationship slightly overestimates Ω_{arag} values while the Juranek et al. (2009) relationship underestimates Ω_{arag} in deeper waters and overestimates Ω_{arag} in shallower waters (Fig. S1).

Application to Regional Time Series

The relationship developed here was applied to three regional time series: ACCESS data (available from 2010 to 2015), Bodega Line data (2012–2015), and BOON mooring data (2014–2015). Parts of the first two datasets (2012–2015) were used in model development and verification where Ω_{arag} could be derived from bottle samples, as described above.

Application of model results allow estimation of Ω_{arag} depth profiles from CTD data and calculation of Ω_{arag} time series from mooring data, thus resolving high-frequency variations and small-scale spatial patterns (Figs. 5–8) as well as hindcasting Ω_{arag} at sites where measurements have been either absent or present at lower temporal or spatial resolution than other hydrographic parameters.

Application of our model to CTD casts from ACCESS cruises reveals spatial variability in on-shelf Ω_{arag}. Transects show the Ω_{arag} saturation horizon (depth at which Ω_{arag} crosses one) shoaling to the east and north in most years, towards the upwelling center at Point Arena (Largier et al. 1993; Figs. 6 and 7). Waters at ACCESS Line 6, near Southeast Farallon Island, are more saturated with respect to aragonite (e.g. Fig. 6), consistent with air-sea interaction and mixing with productive, higher saturation state, surface waters as they flow away from the upwelling center towards and past Point Reyes (Halle and Largier 2011). Interannual variability is also observed in this dataset. For example, a largely undersaturated water column (from a depth of ~ 50–75 m) is observed in 2010 as compared with 2015, along with reduced north-south variability in 2010 (Fig. 7).

The temporal variability in Ω_{arag} depth profiles estimated from Bodega Line data are presented in Fig. 5, showing changes in the Ω_{arag} saturation horizon depth. During winter months, the Ω_{arag} saturation horizon deepens to > 100 m

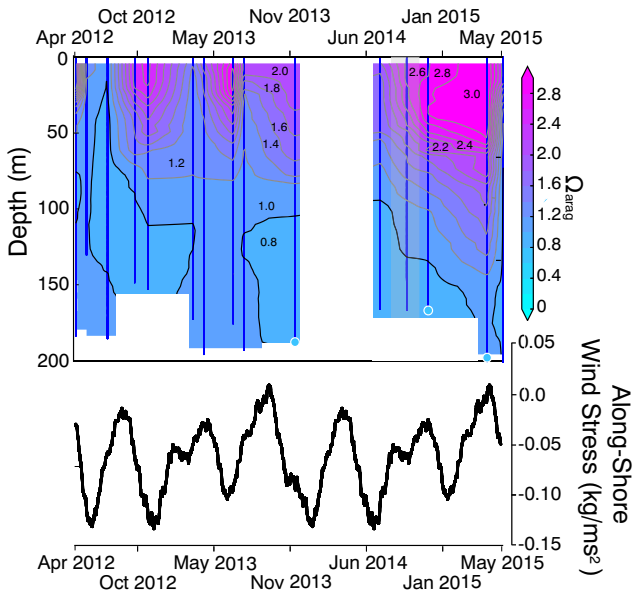

Fig. 5 Reconstructed time series of estimates Ω_{arag} at Bodega Line Station 4 between Spring 2012 and Spring 2015. Temperature, salinity and DO data are from CTD casts, represented by vertical blue lines. The aragonite saturation horizon ($\Omega_{arag} = 1$) is shown in black, with other contours in gray. Between CTD casts, data are linearly interpolated, up to a maximum data gap of 90 days. A CTD cast obtained in September has been demarked with a gray box. Alongshore wind stress with a 10 day running mean is shown below. Where Ω_{arag} has also been calculated by laboratory measurement of pH and alkalinity, this is shown as appropriately colored dots

through the majority of the season. Water undersaturated with respect to aragonite shoals with the onset of upwelling in spring to < 20 m in the spring of 2012. However, the Ω_{arag} saturation horizon remains deeper in the spring of 2014 than in previous years.

Aragonite saturation state was also estimated for high-frequency data from instruments moored at 30 m depth on the nearshore BOON mooring, 1.2 km offshore Bodega Head (Fig. 1). Estimated bottom water Ω_{arag} shows both seasonal and synoptic variability, with low Ω_{arag} values associated with upwelling (stronger upwelling favorable winds and colder water) and higher Ω_{arag} values associated with warmer waters during relaxation (Fig. 8). Synoptic variability is superimposed on a seasonal cycle with high Ω_{arag} values through winter. Although only at one location, these high-frequency data provide a fuller picture of the temporal variability of benthic Ω_{arag}, which is found to be undersaturated ($\Omega_{arag} < 1$) 24% of the time (Fig. 8).

Estimated Ω_{arag} also documents the interannual variability found along the Northern California Margin. For example, summer Ω_{arag} data, both calculated and estimated, at Bodega Line Station 4 in 2014 and 2015 indicates a deeper Ω_{arag} saturation horizon and overall higher Ω_{arag} compared to previous years (Fig. 5). Years with a deeper Ω_{arag} saturation horizon are coincident with oceanographically unusual warm anomalies: the appearance of North Pacific sea surface temperature anomalies that start in late 2013 and continue through 2014 and 2015, overlapping with the onset of the 2015–2016 El Niño.

Discussion

A Regionally and Seasonally Specific Model for Ω_{arag}

Measurements of carbonate chemistry obtained over 4 years along the Northern California margin document a relationship between Ω_{arag}, temperature, and DO that is comparable with relationships developed elsewhere in the CCS but show that Ω_{arag} in this region is not well estimated by the relationships from other regions (Alin et al. 2012; Juranek et al. 2009). In addition to being latitudinally distinct, the relationship between Ω_{arag}, temperature, salinity, and DO may be influenced by the focus on mainly, near-shore and on shelf sites, as well as San Francisco Bay outflow. We find that previously employed parameters (temperature and DO) can be used together with salinity and interactive parameters to construct a more robust, regionally specific predictive model for Ω_{arag}. The inclusion of both salinity and temperature increases the utility of the empirical model across datasets in the region (Table 1), likely as an additional signature of upwelled water masses associated with low Ω_{arag}. Further, salinity may help differentiate between the influence of runoff and San Francisco Bay outflow that is transported northward past

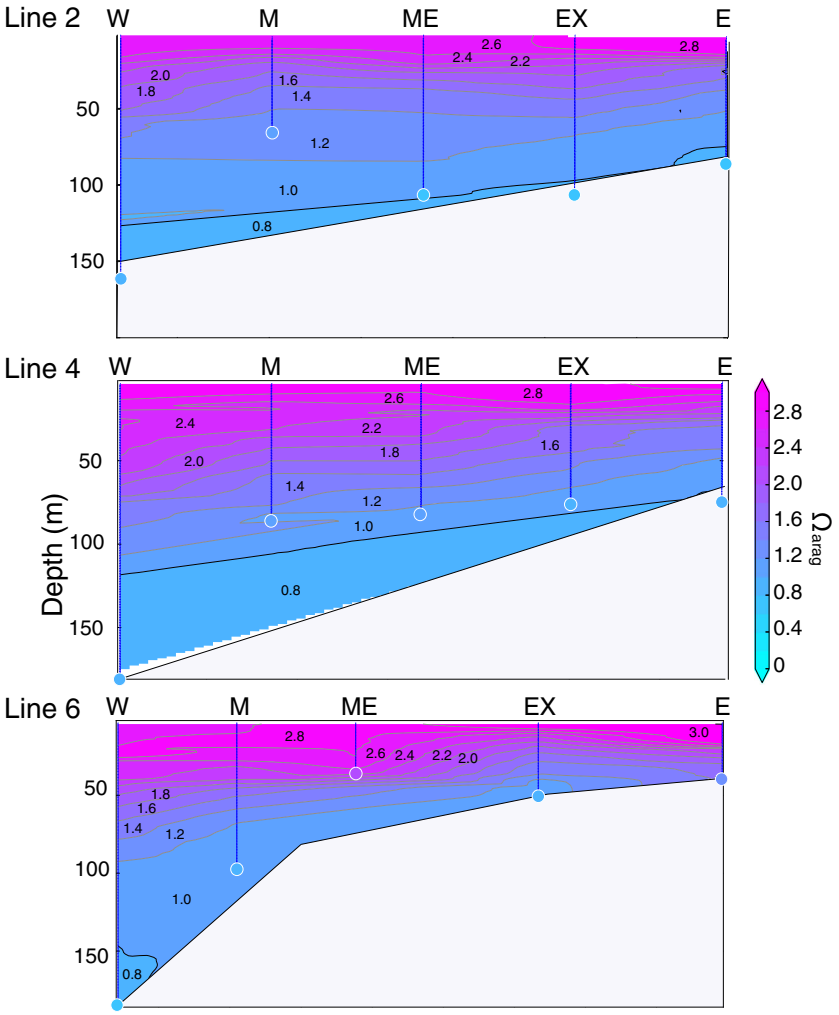

Fig. 6 Reconstructed spatial transects of estimated Ω_{arag} for ACCESS cruise lines 2 (15.5–48.6 km offshore), 4 (13–41.5 km offshore), and 6 (18.2–35.4 km offshore) in July 2015. Temperature, salinity, and DO are from CTD casts for depths > 5 m. The aragonite saturation horizon ($\Omega_{arag} = 1$) is shown in black, with other contours in gray. Vertical blue lines show the CTD casts (temperature, salinity, and DO) from which Ω_{arag} profiles are estimated. Westernmost and easternmost stations of each transect are on the boundaries of the section. Where Ω_{arag} has also been calculated by laboratory measurement of pH and alkalinity, this is shown as appropriately colored points

Point Reyes during periods of relaxation in upwelling winds (Largier et al. 2006; Send et al. 1987). Thus inclusion improves model performance in relation to the Bodega Line data, exclusively collected nearer Bodega Bay (Fig. 1). We documented seasonal variation in model accuracy, with substantial deviations from model predictions in September, when upwelling is generally weaker.

The Association of Low Ω_{arag} with Upwelled Waters

A direct relationship between the inorganic carbon system (including low Ω_{arag}) and upwelled source waters has been shown multiple times elsewhere in the CCS (Alin et al. 2012; Fassbender et al. 2011; Feely et al. 2008; Hales et al. 2005; Juranek et al. 2009). This association is reaffirmed here, first by observation of seasonal shoaling of undersaturated waters in association with the onset of upwelling favorable winds (negative along-shore wind stress; Fig. 5) and second by bottom water observations from the BOON offshore mooring, where denser waters are linked to low Ω_{arag} (Fig. 8). Interestingly, here, we observe aragonite undersaturation in waters with densities as low as 25.2 kg m^{-3} (Fig. 8), notably lower than the densities of deep source waters reported in prior studies associated with $\Omega_{arag} < 1$ (26.2 kg m^{-3}; Feely et al. 2008). The presence of relatively less dense water associated with low Ω_{arag} is especially prominent in July 2014 and is presumably the result of net respiration over the shelf, which is expected to be stronger in sub-surface waters during unusually strong stratification observed in summer 2014, associated with the warm anomaly at that time (see further discussion below; Fig. 8). Such a mechanism has previously implicated in decreasing saturation state in upwelling regions (Fassbender et al. 2011) and is supported by the observation of persistent low DO at the site even as temperatures rise and salinity decreases.

September Data

Shelf DO concentrations are influenced by source water variability associated with upwelling as well as by productivity and respiration in the water column over the shelf. Both influences impact Ω_{arag} proportionally to DO when driven

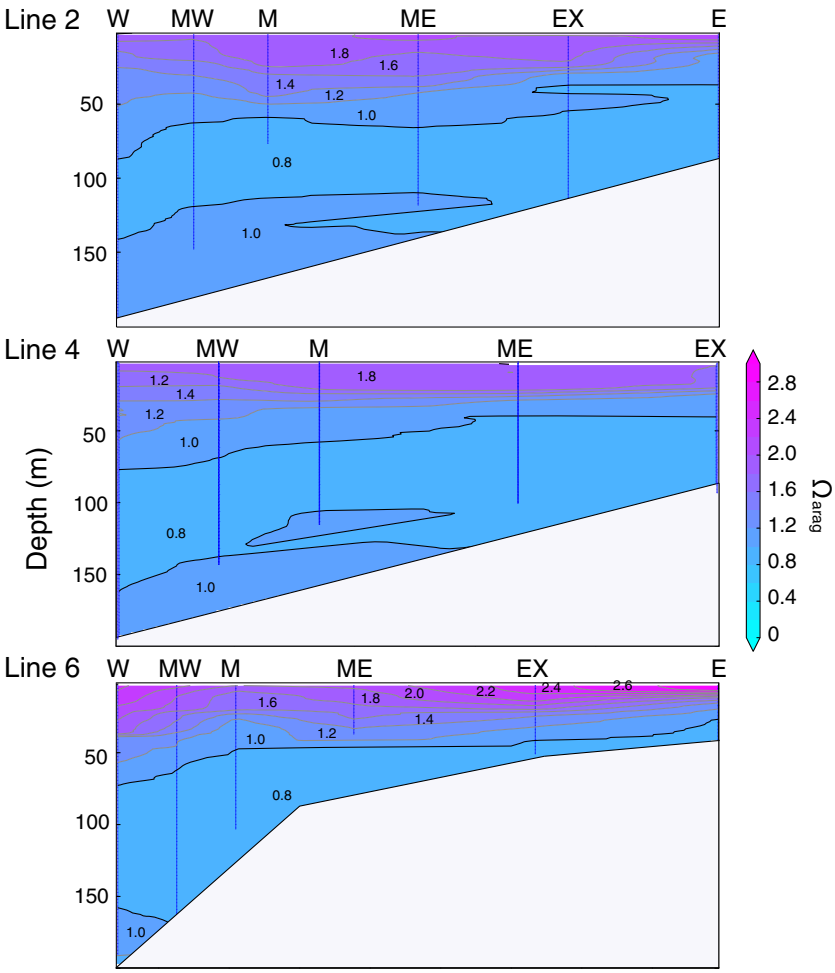

Fig. 7 Reconstructed spatial transects of estimated Ω_{arag} for ACCESS cruise lines 2 (15.5–48.6 km offshore), 4 (13–41.5 km offshore), and 6 (18.2–35.4 km offshore) from July 2010. Temperature, salinity, and DO data are from CTD casts of depth > 5 m (blue). The aragonite saturation horizon ($\Omega_{arag} = 1$) is shown in black, with other contours in gray. Vertical blue lines show the CTD casts (temperature, salinity, and DO) from which Ω_{arag} profiles are estimated. Westernmost and easternmost stations of each transect are on the boundaries of the section

primarily by net respiration (drawdown of oxygen O_2 and increase in CO_2), though not necessarily if dominated by air-sea gas exchange. The poor predictive power of the proposed model during September is due to a change in the relationship between predictors (temperature, salinity, and DO) and Ω_{arag} (Fig. 4). Recognition of such temporal limitations is important in regions where variability in modeling parameters (temperature, salinity, and DO) and their relationship to Ω_{arag} can be influenced by seasonal processes like changes in source waters, the relative importance of productivity/respiration processes, air-sea exchange, or the influence of shelf carbonates. We outline each of these mechanisms further below.

Early fall in Northern California is characterized by a relaxation in upwelling, though upwelling can still occur and the influence of upwelled waters on the shelf may linger, resulting in a mixed upwelling/relaxation signal. Relaxation is accompanied by net northward transport of southerly waters (Kaplan and Largier 2006; Largier et al. 1993, 2006; Send et al. 1987), including waters influenced by San Francisco Bay outflows. Thus, salinity and temperature, in particular (though DO as well), might reflect the duel influence of upwelled and laterally transported surface waters and therefore a more complex relationship with Ω_{arag} than at other times of year and in other places. August and September are also characterized by significant stratification, which limits air-sea exchange to a shallow near-surface layer and by phytoplankton blooms that are dominated by dinoflaggelates and the pseudonitzschia diatom (Paquin 2012). These blooms appear as sub-surface chlorophyll maxima offshore—thus inserting the production effect sub-surface, rather than in the least-dense surface waters, in contrast to diatom-dominated blooms in other seasons. Moreover, if the influence of upwelling-driven productivity outlasts that of upwelled water masses, due to remnant nutrients and the longer lifespans of higher trophic level consumers, this transitional period would be distinct in the relative importance of the primary productivity (high Ω_{arag}) and respiration (low Ω_{arag}) signal compared to upwelling (low Ω_{arag}) in determining local Ω_{arag}. It is also possible that a change in the type of productivity during this period results in altered Redfield C:O ratios.

One additional possibility is the interaction of upwelled waters with shelf sediment carbonates or those in San Francisco Bay. During upwelling season, water masses with low DO and low Ω_{arag} are brought onto the shelf, and as these

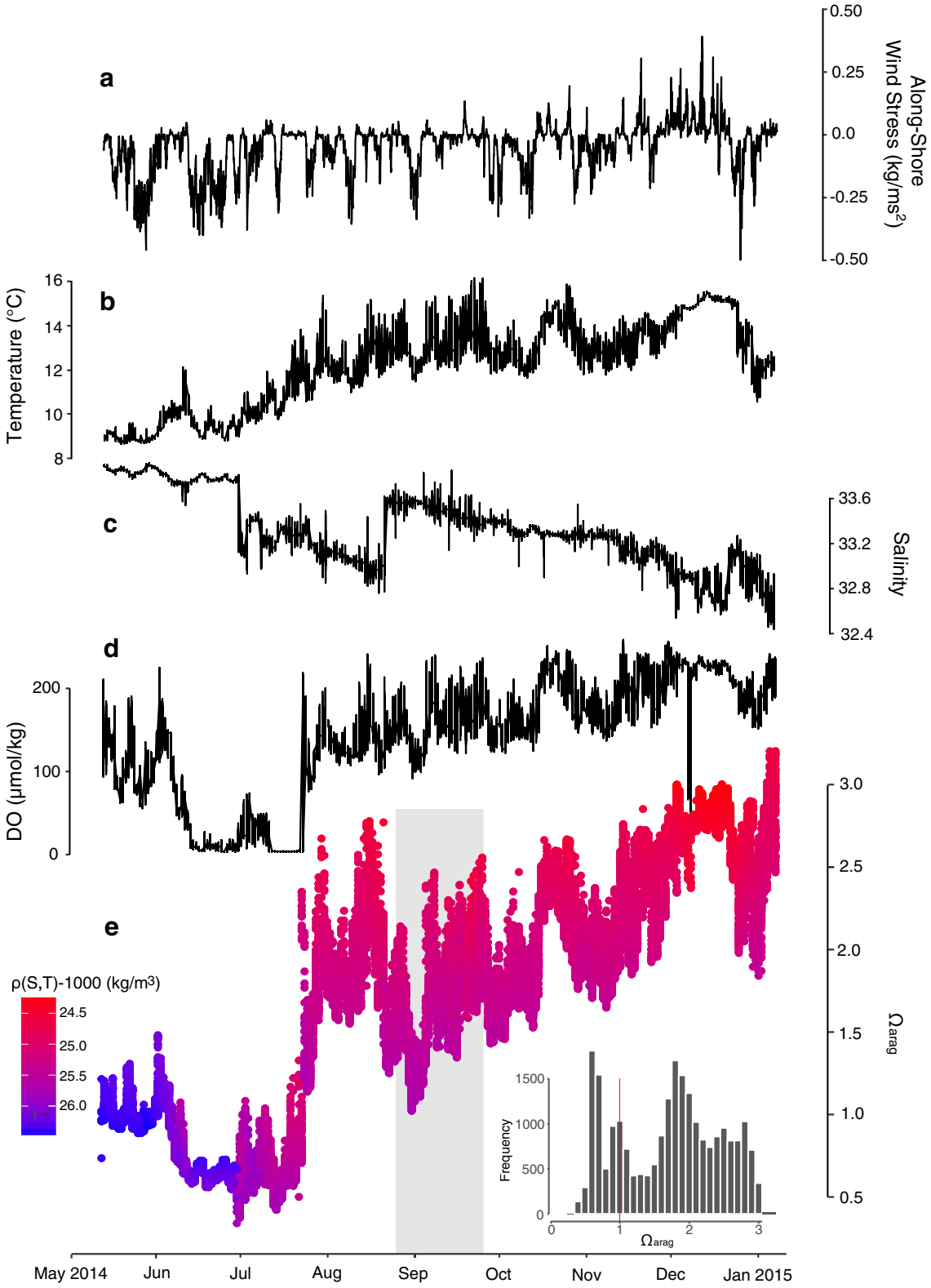

Fig. 8 Observations at 30 m depth on the Bodega Ocean Observing Node (BOON) mooring, located 1 km offshore (Fig. 1). **a** Alongshore wind stress from NDBC46013, **b** temperature, **c** salinity, **d** DO, and **e** estimated Ω_{arag} with water density shown in color. A histogram of estimated Ω_{arag} at the site is shown in the lower right corner, indicating 24% of observations document estimate $\Omega_{arag} < 1$. Data reconstructed during September conditions are indicated by a gray box

water masses have extended contact with the shelf, they may be buffered by dissolution of carbonate shells in the shelf sediments and water column, increasing Ω_{arag}, independent of DO. Such an interaction would be poorly predicted by measured parameters (temperature, salinity, and DO) and could become more pronounced towards the end of upwelling season, when increased stratification and decreased upwelling would allow corrosive upwelled water masses increased contact time at the sediment-water interface and within pore waters. In fact, while the expected proportional relationship between total CO_2 and DO is present in all ACCESS data collected (May–September), it is more robust in May–July (R^2 = 0.64) than in September (R^2 = 0.49) and the measured Ω_{arag} during September is indeed often higher than estimated by our model. One or more of these mechanisms could account for the failure of the upwelling-driven model to estimate September Ω_{arag} values. Continued data collection may yield a September-specific model that better represents these mechanisms.

Oceanographic Variability

From late 2013 to late 2015, the North Pacific experienced a marine heat wave, a warm anomaly popularly called "The Blob" (Bond et al. 2015). Sea surface temperature anomalies were accompanied by a switch to a positive Pacific Decadal Oscillation (PDO) phase (Leising et al. 2015) which may have precipitated a series of unusual global climate patterns (Lee et al. 2015), including reduced upwelling in the Central CCS in 2014 (Gentemann et al. 2017; Leising et al. 2015). Marine heat waves are statistically common in the Eastern North Pacific with a frequency of one every 4 years (Scannell et al. 2016). However, "The Blob" is notable for being the most extreme such anomaly observed since at least 1980 (Bond et al. 2015). It was accompanied by numerous, productivity shifts and species observation ranging from unusual sightings of seabirds and *Vellela vellela* to temporal and range shifts in valuable fisheries catches including skipjack tuna and sockeye salmon in the Pacific Northwest (Bond et al. 2015; Whitney 2015) and along the California coast (Leising et al. 2015). "The Blob" was also associated with a reduction in upwelling at these latitudes (Leising et al. 2015). Coastal upwelling occurred off Northern California in spring 2014 and 2015, with anomalously warm surface waters only being sustained after May (Gentemann et al. 2017), accompanied by anomalously strong stratification. Our observations show this upwelling in early 2014 (Fig. 8) and early 2015 (Fig. 5), and during the summer and fall 2014, although Ω_{arag} estimated at the BOON mooring (Fig. 8) is lower than that from shipboard measurements (Fig. 5). This is consistent with a shoreward shoaling of the Ω_{arag} saturation horizon as seen in cross-shelf transects (Fig. 6; Fig. 7), due to shoaling of upwelled waters and the effect of net respiration as waters move onshore.

El Niño events have been associated with an overall decrease in and shift to a later onset of upwelling at the latitudes of our study location (Bograd et al. 2009; Jacox et al. 2015). In fall 2015, El Niño conditions were observed in the Eastern Pacific (Stramma et al. 2016), following effects of the 2014–2015 marine heat wave. This explains the deeper Ω_{arag} saturation horizon observed in 2015, due to a regional change in upwelling. Given a demonstrated link between El Niño and upwelling in this region and upwelling and Ω_{arag} more broadly, an association between ENSO and Ω_{arag} saturation horizon depth is likely to be observered again in future years. Thus, the records presented here illustrate an important link between interannual and decadal scale variability in Pacific climate and shelf exposure to aragonite undersaturated waters. A deeper Ω_{arag} saturation horizon is expected to persist in conjunction with reduced or late season upwelling during marine heat waves and El Niño events.

By contrast, a shallower summer Ω_{arag} saturation horizon depth would be associated with stronger upwelling, which appears to be intensifying off California (García-Reyes and Largier 2012) and also during La Niña conditions. The latter is apparent in transects from the July ACCESS Cruises when years with weak upwelling (2015) and strong upwelling (2010) are compared (Fig. 6; Fig. 7). In 2015, waters highly saturated with respect to aragonite are present at the surface, with a relatively deep summer Ω_{arag} saturation horizon, similar to observations from Bodega Line Station 4 during the same year (Figs. 5 and 6). By contrast, in 2010, the Ω_{arag} saturation horizon depth is shallower and less spatially variable than in July 2015 (Fig. 7). During this La Niña year, the water column is largely undersaturated with respect to aragonite across ACCESS transects, with the Ω_{arag} saturation horizon depth shoaling to < 50 m on the shoreward end of all lines (Fig. 7).

Given the relatively short extent of this 6 year time series, it is unclear how unusual the deep Ω_{arag} saturation horizon observed in 2014–2015 is for the Northern California region. However, the anomalies seen in these years are representative of a type of interannual variability in Ω_{arag} that has been difficult to capture on a regional scale. Because calibration data were collected both prior to and during the anomalous years of 2014 and 2015, there is confidence in the ability of this regional model to detect an interannual diversity of Ω_{arag} regimes.

Community Exposure

These time series show the extent to which shelf communities in the central CCS are already exposed to aragonite undersaturated conditions. For example, sensors on the shallow BOON mooring, located 1 km offshore at a water depth of 30 m (Fig. 1), were exposed to $\Omega_{arag} < 1$ waters for 24% of the time in 2014. Non-motile shelf communities would thus have been exposed to undersaturated

conditions for roughly a quarter of the year, beginning with the spring shoaling of the Ω_{arag} saturation horizon, and to strongly aragonite undersaturated ($\Omega_{arag} < 0.5$) conditions in June and July (Fig. 8). Given that this was an anomalous year, with the Ω_{arag} saturation horizon deeper offshore than in preceding years (Fig. 5), estimated Ω_{arag} at the BOON mooring may in fact represent a shorter duration or intensity of aragonite undersaturation than would be expected at the site in other years. A greater understanding of exposure thresholds and tolerances in these specific communities is imperative for evaluating the risks of the combined threat of global OA and intensified upwelling.

Conclusions

We present an empirical relationship for estimating Ω_{arag} in waters off Northern California. The relationship relies on measurements of temperature, salinity, and DO and can be applied to regional datasets to increase the temporal and spatial resolution of ocean acidification monitoring in the region. From estimated Ω_{arag}, we can begin to quantify seasonal and interannual variability in the upwelling-associated shoaling of the Ω_{arag} saturation horizon. Documentation of this variability provides an essential baseline in a highly variable region where both ocean-wide decreases in Ω_{arag} and changes in upwelling strength will impact marine communities. Shelf communities in the area as shallow as 30 m already experience extended exposure to waters undersaturated with respect to aragonite and thus may be particularly sensitive to ongoing changes.

Acknowledgements We would like to thank D. Dann, M.G. Susner, D. Lipski, J. Roletto, and the crew of the R/V *Fulmar* for assistance in the field and A. Ninokawa and J. Hosfelt for laboratory support. The authors would also like to thank E. Sanford, J. Hower, M. Elliott, and N. Karnovsky.

All oceanographic data are available upon request from the Bodega Marine Laboratory (Bodega Line/BOON) and Point Blue (ACCESS: http://www.pointblue.org/datasharing).

Funding Information This work was supported by the National Science Foundation OCE No. 144451 to TMH and California Sea Grant R/HCME-04 to JLL. Support for BOON and the Bodega Line data was received from UC Davis, Sonoma County Water Agency, and the Central and Northern California Ocean Observing System (CeNCOOS).

This research was supported in part by the Applied California Current Ecosystem Studies (ACCESS) partnership, a continuing collaboration between Point Blue Conservation Science, the Greater Farallones National Marine Sanctuary, and Cordell Bank National Marine Sanctuary. The authors thank the Angell Family Foundation, Bently Foundation, Bonnel Cove Foundation, Boring Family Foundation, Elinor Paterson Baker Trust, Faucett Catalyst Fund, Firedoll Foundation, Hellman Family Foundation, Moore Family Foundation, Pacific Life Foundation, Susie Tompkins Buell Foundation, Wendy P. McCaw Foundation, Thelma Doelger Trust, and the many Point Blue donors who have helped fund ACCESS work over the years. This is Point Blue Conservation Science contribution number 2106 and a contribution of Bodega Marine Laboratory.

References

Akaike, H. 1974. A new look at the statistical model identification. *IEEE Transactions on Automatic Control* 19 (6): 716–723. https://doi.org/10.1109/TAC.1974.1100705.

Alin, S.R., R.A. Feely, A.G. Dickson, J.M. Hernández-Ayón, L.W. Juranek, M.D. Ohman, and R. Goericke. 2012. Robust empirical relationships for estimating the carbonate system in the southern California Current System and application to Cal COFI hydrographic cruise data (2005–2011). *Journal of Geophysical Research: Oceans* 117 (5): C05033.

Bakun, A. 1990. Global climate change and intensification of coastal ocean upwelling. *Science* 247 (4939): 198–201. https://doi.org/10.1126/science.247.4939.198.

Bakun, A., B. Black, S.J. Bograd, M. Garcia-Reyes, A. Miller, R. Rykaczewski, and W. Sydeman. 2015. Anticipated effects of climate change on coastal upwelling ecosystems. *Current Climate Change Reports* 1 (2): 85–93. https://doi.org/10.1007/s40641-015-0008-4.

Bograd, S.J., I. Schroeder, N. Sarkar, X. Qiu, W.J. Sydeman, and F.B. Schwing. 2009. Phenology of coastal upwelling in the California Current. *Geophysical Research Letters* 36 (1): L01602.

Bond, N.A., M.F. Cronin, H. Freeland, and N. Mantua. 2015. Causes and impacts of the 2014 warm anomaly in the NE Pacific. *Geophysical Research Letters* 42 (9): 3414–3420. https://doi.org/10.1002/2015GL063306.

Broecker, W.S., and T.H. Peng. 1982. Tracers in the Sea. Lamont-Doherty Geological Observatory, Columbia University.

Caldeira, K., and M.E. Wickett. 2003. Oceanography: anthropogenic carbon and ocean pH. *Nature* 425 (6956): 365–365. https://doi.org/10.1038/425365a.

Canadell, J.G., C. Le Quéré, M.R. Raupach, C.B. Field, E.T. Buitenhuis, P. Ciais, T.J. Conway, N.P. Gillett, R.A. Houghton, and G. Marland. 2007. Contributions to accelerating atmospheric CO2 growth from economic activity, carbon intensity, and efficiency of natural sinks. *Proceedings of the National Academy of Sciences* 104 (47): 18866–18870. https://doi.org/10.1073/pnas.0702737104.

Canty, A. and B. Ripley. 2016. Boot: Bootstrap R (S-Plus) functions. R package version 1.3–18.

Chan, F., J.A. Barth, C.A. Blanchette, R.H. Byrne, F. Chavez, O. Cheriton, R.A. Feely, G. Friederich, B. Gaylord, T. Gouhier, S. Hacker, T. Hill, G. Hofmann, M.A. McManus, B.A. Menge, K.J. Nielson, A. Russell, E. Sanford, J. Sevadjian, and L. Washburn. 2017. Persistent spatial structuring of coastal ocean acidification in the California Current System. *Scientific Reports* 7 (1): 2526. https://doi.org/10.1038/s41598-017-02777-y.

Dickson, A.G. 1990. Thermodynamics of the dissociation of boric acid in synthetic seawater from 273.15 to 318.15 K. *Deep-Sea Research* 37: 755–766.

Dickson, A.G., C.L. Sabine and J.R. Christian. 2007. SOP 6b: determination of the pH of sea water using the indicator dye m-cresol purple. Guide to best practices for ocean CO_2 measurements. Sidney: North Pacific Marine Science Organization.

Doney, S.C., V.J. Fabry, R.A. Feely, and J.A. Kleypas. 2009. Ocean acidification: the other CO_2 problem. *Annual Review of Marine Science* 1 (1): 169–192. https://doi.org/10.1146/annurev.marine.010908.163834.

Fabry, V.J., B.A. Seibel, R.A. Feely, and J.C. Orr. 2008. Impacts of ocean acidification on marine fauna and ecosystem processes. *ICES Journal of Marine Science: Journal du Conseil* 65 (3): 414–432. https://doi.org/10.1093/icesjms/fsn048.

Fassbender, A.J., C.L. Sabine, R.A. Feely, C. Langdon, and C.W. Mordy. 2011. Inorganic carbon dynamics during Northern California coastal upwelling. *Continental Shelf Research* 31 (11): 1180–1192. https://doi.org/10.1016/j.csr.2011.04.006.

Feely, R.A., C.L. Sabine, K. Lee, W. Berelson, J. Kleypas, V.J. Fabry, and F.J. Millero. 2004. Impact of anthropogenic CO_2 on the $CaCO_3$ system in the oceans. *Science* 305 (5682): 362–366. https://doi.org/10.1126/science.1097329.

Feely, R.A., S.C. Doney, and S.R. Cooley. 2009. Ocean acidification: present conditions and future changes in a high-CO_2 world. *Oceanography* 22 (4): 36–47. https://doi.org/10.5670/oceanog.2009.95.

Feely, R.A., C.L. Sabine, J.M. Hernandez-Ayon, D. Ianson, and B. Hales. 2008. Evidence for upwelling of corrosive "acidified" water onto the continental shelf. *Science* 320 (5882): 1490–1492. https://doi.org/10.1126/science.1155676.

Feely, R.A., S.R. Alin, B. Carter, N. Bednarsek, B. Hales, F. Chan, T.M. Hill, B. Gaylord, E. Sanford, R.H. Byrne, C.L. Sabine, D. Greeley, and L. Juranek. 2016. Chemical and biological impacts of ocean acidification along the west coast of North America: Estuarine. *Coastal and Shelf. Science* 183: 260–270. https://doi.org/10.1016/j.ecss.2016.08.043.

García-Reyes, M., and J. Largier. 2010. Observations of increased wind-driven coastal upwelling off Central California. *Journal of Geophysical Research* 115: C04011. https://doi.org/10.1029/2009JC005576.

García-Reyes, M., and J.L. Largier. 2012. Seasonality of coastal upwelling off central and northern California: New insights, including temporal and spatial variability. *Journal of Geophysical Research Oceans* 117 (3): C03028.

García-Reyes, M., W.J. Sydeman, D.S. Schoeman, R.R. Rykaczewski, B.A. Black, A.J. Smit, and S.J. Bograd. 2015. Under pressure: climate change, upwelling, and eastern boundary upwelling ecosystems. *Frontiers in Marine Science* 2: 109.

Gay, P.S., and T.K. Chereskin. 2009. Mean structure and seasonal variability of the poleward undercurrent off southern California. *Journal of Geophysical Research* 114: C02007. https://doi.org/10.1029/2008JC004886.

Gentemann, C.L., M.R. Fewings, and M. Garcia-Reyes. 2017. Satellite sea surface temperatures along the West Coast of the United States during the 2014–2016 northwest Pacific marine heat wave. *Geophysical Research Letters* 4 (1): 312–319.

Gruber, N., C. Hauri, Z. Lachkar, D. Loher, T.L. Frölicher, and G. Plattner. 2012. Rapid progression of ocean acidification in the California Current System. *Science* 337 (6091): 220–223. https://doi.org/10.1126/science.1216773.

Hales, B., T. Takahashi, and L. Bandstra. 2005. Atmospheric CO_2 uptake by a coastal upwelling system. *Global Biogeochemical Cycles* 19: GB1009.

Halle, C.M., and J.L. Largier. 2011. Surface circulation downstream of the Point Arena upwelling center. *Continental Shelf Research* 31 (12): 1260–1272. https://doi.org/10.1016/j.csr.2011.04.007.

Hauri, C., N. Gruber, M. Vogt, S.C. Doney, R.A. Feely, Z. Lachkar, A. Leinweber, A.M.P. McDonnell, M. Munnich, and G.K. Plattner. 2013. Spatiotemporal variability and long-term trends of ocean acidification in the California Current System. *Biogeosciences* 10 (1): 193–216. https://doi.org/10.5194/bg-10-193-2013.

Harris, K.E., M.D. DeGrandpre, and B. Hales. 2013. Aragonite saturation state dynamics in a coastal upwelling zone. *Geophysical Research Letters* 40 (11): 2720–2725. https://doi.org/10.1002/grl.50460.

Hickey, B.M. 1979. The California current system—Hypotheses and facts. *Progress in Oceanography* 8e(4): 191–279.

Hickey, B.M. 1998. Coastal oceanography of western North America from the tip of Baja California to Vancouver Island. In *The global Coastal Ocean: Regional studies and syntheses*, ed. A.R. Robinson and K.H. Brink, vol. vol. 11. New York: Wiley.

Hofmann, G.E., J.E. Smith, K.S. Johnson, U. Send, L.A. Levin, F. Micheli, A. Paytan, N.N. Price, B. Peterson, Y. Takeshita, P.G. Matson, E.D. Crook, K.J. Kroeker, M.C. Gambi, E.B. Rivest, C.A. Frieder, P.C. Yu, and T.R. Martz. 2011. High-frequency dynamics of ocean pH: a multi-ecosystem comparison. *PLoS One* 6 (12): e28983. https://doi.org/10.1371/journal.pone.0028983.

Huyer, A. 1998. Coastal upwelling in the California Current System. *Progress in Oceanography* 12 (3): 259–284. https://doi.org/10.1016/0079-6611(83)90010-1.

Huyer, A., J. Barth, P. Kosro, R. Shearman, and R. Smith. 1998. Upper-Ocean water mass characteristics of the California current, summer 1993. *Deep Sea Research Part II* 45 (8–9): 1411–1442.

Jacox, M.G., J. Fiechter, A.M. Moore, and C.A. Edwards. 2015. ENSO and the California Current coastal upwelling response. *Journal of Geophysical Research: Oceans* 120 (3): 1691–1702. https://doi.org/10.1002/2014JC010650.

Juranek, L.W., R.A. Feely, W.T. Peterson, S.R. Alin, B. Hales, K. Lee, C.L. Sabine, and J. Peterson. 2009. A novel method for determination of aragonite saturation state on the continental shelf of central Oregon using multi-parameter relationships with hydrographic data. *Geophysical Research Letters* 36 (24): L24601. https://doi.org/10.1029/2009GL040778.

Kaplan, D.M., and J.L. Largier. 2006. HF radar-derived origin and destination of surface waters off Bodega Bay, California. *Deep-Sea Research II* 53 (25-26): 2906–2930. https://doi.org/10.1016/j.dsr2.2006.07.012.

Kelly, M.W., J.L. Padilla- Gamiño, and G.E. Hofmann. 2013. Natural variation and the capacity to adapt to ocean acidification in the keystone sea urchin *Strongylocentrotus purpuratus*. *Global Change Biology* 19 (8): 2536–2546. https://doi.org/10.1111/gcb.12251.

Kleypas, J.A., R.W. Buddemeier, D. Archer, J.-P. Gattuso, C. Langdon, and B.N. Opdyke. 1999. Geochemical consequences of increased atmospheric carbon dioxide on coral reefs. *Science* 284 (5411): 118–120. https://doi.org/10.1126/science.284.5411.118.

Largier, J.L., B.A. Magnell, and C.D. Winant. 1993. Subtidal circulation over the Northern California shelf. *Journal of Geophysical Research* 98 (C10): 18147–18179. https://doi.org/10.1029/93JC01074.

Largier, J.L., C.A. Lawrence, M. Roughan, D.M. Kaplan, E.P. Dever, C.E. Dorman, R.M. Kudela, S.M. Bollens, F.P. Wilkerson, R.C. Dugdale, L.W. Botsford, N. Garfield, B. Kuebel-Cervantes, and D. Koracin. 2006. WEST: a Northern California study of the role of wind-driven transport in the productivity of coastal plankton communities. *Deep Sea Research II* 53 (25–26): 2833–2849. https://doi.org/10.1016/j.dsr2.2006.08.018.

Lee, M.Y., C.C. Hong, and H.H. Hsu. 2015. Compounding effects of warm sea surface temperature and reduced sea ice on the extreme circulation over the extratropical North Pacific and North America during the 2013–2014 boreal winter. *Geophysical Research Letters* 42 (5): 1612–1618. https://doi.org/10.1002/2014GL062956.

Leising, A.W., I.D. Schroeder, S.J. Bograd, J. Abell, R. Durazo, G. Gaxiola-Castro, E.P. Bjorkstedt, J. Field, K. Sakuma, and R.R. Robertson. 2015. State of the California Current 2014-15: Impacts of the Warm-Water "Blob." CalCOFI Report, 56:31–68.

Lynn, R.J., and J.J. Simpson. 1987. The California Current System: the seasonal variability of its physical characteristics. *Journal of Geophysical Research: Oceans* 92 (12): 12947–12966. https://doi.org/10.1029/JC092iC12p12947.

Meinvielle, M., and G.C. Johnson. 2013. Decadal water-property trends in the California Undercurrent, with implications for ocean acidification. *Journal of Geophysical Research: Oceans* 118 (12): 6687–6703. https://doi.org/10.1002/2013JC009299.

Millero, F.J. 2010. Carbonate constants for estuarine waters. *Marine and Freshwater Research* 61: 139–142.

Mote, P.W., and N.J. Manuta. 2002. Coastal upwelling in a warmer future. *Geophysical Research Letters* 29 (23): 2138–2142.

Orr, J.C., V.J. Fabry, O. Aumont, L. Bopp, S.C. Doney, R.A. Feely, A. Gnanadesikan, N. Gruber, A. Ishida, F. Joos, R.M. Key, K. Lindsay, E. Maier-Reimer, R. Matear, P. Monfray, A. Mouchet, R.G. Najjar, G.-K. Plattner, K.B. Rodgers, C.L. Sabine, J.L. Sarmiento, R. Schlitzer, R.D. Slater, I.J. Totterdell, M.-F. Weirig, Y. Yamanaka, and A. Yool. 2005. Anthropogenic ocean acidification over the twenty-first century and its impact on calcifying organisms. *Nature* 437 (7059): 681–686. https://doi.org/10.1038/nature04095.

Parker, L., P.M. Ross, and W.A. O'Connor. 2011. Populations of the Sydney rock oyster, *Saccostrea glomerata*, vary in response to ocean acidification. *Marine Biology* 158 (3): 689–697. https://doi.org/10.1007/s00227-010-1592-4.

Paquin, A. 2012. The green thread: seasonal and event scale forcing of phytoplankton abundance and taxonomic composition in the surfzone of open-coast, rocky shore. MS Thesis. Sonoma State University. http://hdl.handle.net/10211.3/121491

Pennington, T.J., and F.P. Chavez. 2000. Seasonal fluctuations of temperature, salinity, nitrate, chlorophyll and primary production at station H3/M1 over 1989–1996 in Monterey Bay, California. *Deep Sea Research Part II* 47 (5–6): 947–973.

Pickard, G.L. 1964. *Descriptive physical oceanography*. New York: Pergamon.

Pierce, S.D., J.A. Barth, R.K. Shearman, and A.Y. Erofeev. 2012. Declining oxygen in the Northeast Pacific. *Journal of Physical Oceanography* 42: 495–501.

R Core Team. 2013. *A language and environment for statistical computing*. Vienna: Austria.

Reid, J.L., G.I. Roden, and J.G. Wyllie. 1958. *Studies of the California current system, CalCOFI Prog. Rep. 7–1-56 to 1–1-58*, 27–56. Sacramento: Department of Fish and Game.

Robbins, L.L., M.E. Hansen, J.A. Kleypas and S.C. Meylan. 2010. CO2calc—a user-friendly seawater carbon calculator for Windows, Max OS X, and iOS (iPhone). Reston: U.S. Geological Survey.

Sabine, C.L., R.A. Feely, N. Gruber, R.M. Key, K. Lee, J.L. Bullister, R. Wanninkhof, C. Wong, D.W. Wallace, and B. Tilbrook. 2004. The oceanic sink for anthropogenic CO_2. *Science* 305 (5682): 367–371. https://doi.org/10.1126/science.1097403.

Sabine, C.L., and R.A. Feely. 2007. The oceanic sink for carbon dioxide. In *Greenhouse gas sinks*, ed. D. Reay et al., 31–49. Oxfordshire, U.K.: CABI. https://doi.org/10.1079/9781845931896.0031.

Send, U., R.C. Beardsley, and C.D. Winant. 1987. Relaxation from upwelling in the Coastal Ocean Dynamics Experiment. *Journal of Geophysical Research* 92 (C2): 1683–1698. https://doi.org/10.1029/JC092iC02p01683.

Scannell, H.A., A.J. Pershing, M.A. Alexander, A.C. Thomas, and K.E. Mills. 2016. Frequency of marine heatwaves in the North Atlantic and North Pacific since 1950. *Geophysical Research Letters* 43 (5): 2069–2076. https://doi.org/10.1002/2015GL067308.

Snyder, M.A., L.C. Sloan, N.S. Diffenbaugh, and J.L. Bell. 2003. Future climate change and upwelling in the California Current. *Geophysical Research Letters* 30 (15): 1823.

Stramma, L., T. Fischer, D.S. Grundle, G. Krahmann, H.W. Bange, and C.A. Marandino. 2016. Transition to El Niño conditions in the eastern tropical Pacific in October 2015. *Ocean Science* 12 (4): 861–873. https://doi.org/10.5194/os-12-861-2016.

Sverdrup, H.U., R.H. Fleming, and M.W. Johnson. 1942. *The oceans, their physics, chemistry, and general biology*. New York: Prentice Hall.

Sydeman, W., M. García-Reyes, D. Schoeman, R. Rykaczewski, S. Thompson, B. Black, and S. Bograd. 2014. Climate change and wind intensification in coastal upwelling ecosystems. *Science* 345 (6192): 77–80. https://doi.org/10.1126/science.1251635.

Thomson, R.E., and M.V. Krassovski. 2010. Poleward reach of the California undercurrent extension. *Journal of Geophysical Research* 115: C09027. https://doi.org/10.1029/2010JC006280.

Varela, R., I. Álvarez, F. Santos, M. deCastro, and M. Gómez-Gesteira. 2015. Has upwelling strengthened along worldwide coasts over 1982–2010? *Scientific Reports* 5 (1): 10016. https://doi.org/10.1038/srep10016.

Walther, K., K. Anger, and H.-O. Pörtner. 2010. Effects of ocean acidification and warming on the larval development of the spider crab *Hyas araneus* from different latitudes (54 vs. 79 N). *Marine Ecology Progress Series* 417: 159–170. https://doi.org/10.3354/meps08807.

Wang, D., T.C. Gouhier, B.A. Menge, and A.R. Ganguly. 2015. Intensification and spatial homogenization of coastal upwelling under climate change. *Nature* 518 (7539): 390–394. https://doi.org/10.1038/nature14235.

Whitney, F.A. 2015. Anomalous winter winds decrease 2014 transition zone productivity in the NE Pacific. *Geophysical Research Letters* 42 (2): 428–431. https://doi.org/10.1002/2014GL062634.